11th World Congress on Computational Mechanics (WCCM XI)
5th European Conference on Computational Mechanics (ECCM V)
6th European Conference on Computational Fluid Dynamics (ECFD VI)
E. Oñate, J. Oliver and A. Huerta (Eds)

EXPERIMENTAL AND NUMERICAL STUDIES OF LARGE STEEL PLATES SUBJECTED TO HIGH PRESSURE LOADING

S. BÉLANGER [*1], S. BRODEUR [2], J.B. DASTOUS [3], N. SOUCY [4]

[1, 3, 4] Institut de recherche d'Hydro-Québec
1800, blvd Lionel-Boulet, Varennes, Qc, Canada
[1] e-mail: belanger.sylvain@ireq.ca, www.hydroquebec.com
[3]email: dastous.jean-bernard@ireq.ca, www.hydroquebec.com
[4]email: soucy.nathalie@ireq.ca, www.hydroquebec.com

[2]ABB Canada
1600 blvd Lionel-Boulet, Varennes, Qc, Canada
e-mail: samuel.s.brodeur@ca.abb.com, www.abb.ca

Key Words: *Large deflections, Tearing of plates, HSLA steel, Nonlinear finite element analysis*

Abstract. Low impedance faults occurring in power transformers produce electrical arcs that vaporize surrounding oil, leading in some cases to rapid increases of pressure inside. To investigate the behavior of large steel plates that make up a transformer tank, an experimental setup was built to pressurize at small strain rates models of such plates until ductile failure. The experimental results are reported and compared with non linear implicit finite element simulations.

1 INTRODUCTION

There are few studies investigating the effect of pressure loading of large steel plate at a small strain rate leading to the rupture [1]. The majority of the reported studies investigated the dynamic loading of relatively small exposed area on plates where short duration air-blast loadings were mainly achieved using explosives to produce a high strain rate. The first objective of the present study was to produce tearing of plates with low strain to generate one of the three typical failure modes observed by Menkes and Opat [2] : large plastic deformation without failure (Mode I), tensile tearing at the supports (Mode II) and transverse shear at the supports (Mode III).

The experimental results were used to validate three-dimensional static nonlinear finite element models (FEM). The effect of mesh size upon the predicted failure response was evaluated using a convergence study performed in the region of interest of the plate [3]. This established a minimum mesh size to replicate the tearing of the plate with accuracy. Nurick et al. [4] studied the importance of the boundary conditions on plate's response where the machining of a radius on the flange alleviated the indentation. This radius also produced a thinning process similar to the uni-axial bar test and increased the midpoint deflection. The

flange and the support plates must then be included in the finite element model to lessen the stress singularities occurring at the restrained edges as demonstrated by Sinclair [5] and Yuan et al. [6].

2 EXPERIMENTAL METHOD

An experimental test rig was built to simulate pressure rises occurring in oil filled power transformer to investigate their influences on large plates. The setup allowed the loading of plates measuring 2340 mm by 1510 mm designed to reproduce clamped boundary conditions on a rigid tank. Tests were performed on five CSA G40.21 50W flat plates with thickness of 4.76 mm. The material properties and the true stress-true strain curve were characterized from standard uni-axial tensile tests on flat specimens. The results are reported in table 1 where the subscripts *y*, *u* and *f* represent respectively the yield, ultimate and failure values of true stress (σ) and true strain (ε).

Table 1: Material properties of CSA G40.21 50W steel

Test	Speed (mm/min)	Strain (s^{-1})	E (GPa)	σ_y (MPa)	σ_u (MPa)	ε_f (%)
a	2.4	0.0007	194	409	655	14.2
b	2.4	0.0007	181	409	666	16.6

Uniform loading was achieved until failure occurred on the tested item by two different methods. For test No. 1 to 4, a hydraulic pump filled the tank with water and monotonically increased the static pressure while test item No. 5 was loaded with pressurized air. Water or air tightness was achieved by bolting the plate between the flange and a rubber gasket to the tank with 36 bolts. Two pressure transducers recorded the internal pressure.

The flange had a radius of 3.5 mm at the bottom edge and had been stiffened for test No. 3 to 5 by increasing its thickness from 25.4 mm to 50.8 mm and its width from 152 mm to 203 mm. Bolt size was then increased from 1½ in. to 2 in. diameter. It thus reduced the exposed area from 3.01 m^2 to 2.83 m^2. This modification allowed the installation of strain gage at the site of peak strain to avoid interference with the rubber gasket under the plate.

Strain gages installed on the top and bottom (figure 1) of the plate monitored the deformation. The selected gages enabled strain measurement in the post-yield range at value higher than 10%. The integration effect of the strain gage inherently underestimates the peak strain when mounted in a high stress gradient area. Two types of strain gages were used: Vishay Precision Group® EP-08-250RD-350 with a grid size of 6.35 by 3.05 mm and an elongation range of 15 to 20% and TML Tokyo Sokki® YEFRA-2 with grid size of 2.0 by 1.8 mm and an elongation range of 10 to 15%. Curing of the adhesive for the EP-08-250RD-350 strain gage is required to achieve full elongation capability.

A laser distance sensor recorded the midpoint deflection and the lateral displacement of the plate. The lateral displacements of the flange and the tank top flange were measured with DC LVDT displacement transducers.

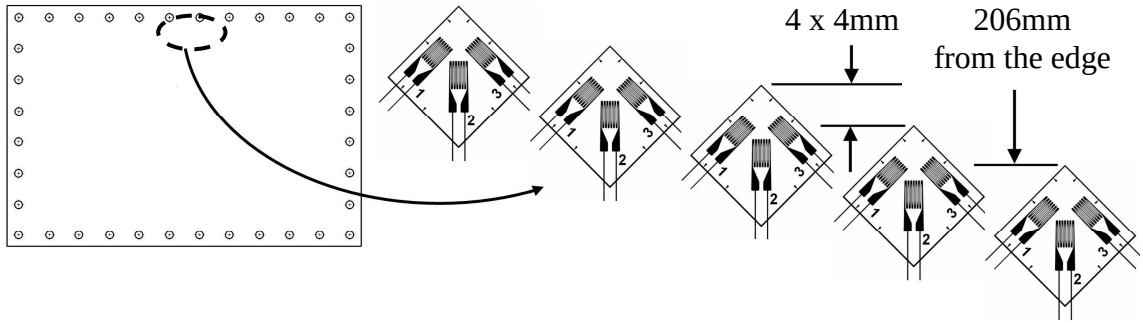

Figure 1: Position of the YEFRA-2 strain gages on the bottom side of plate No. 5

3 EXPERIMENTAL RESULTS

The evolution of the displacement at the plates' midpoint against the internal pressure of the tank shown in figure 2 indicates that higher pressure is required to cause failure of the plates for the 203 mm wide flange with reduced exposed area (tests No. 3, 4 and 5, empty symbols) compared to the 152 mm wide flange (tests No. 1 and 2, filled symbols). Table 2 summarizes the measured results at failure for all the tests. The four water-pressurized loading all produce Mode II failure with partial tearing of the plate on one side as shown in figure 3. There exists a good consistency of the tearing length for the water pressurized plates. Air pressure loading (test No. 5) causes the complete tearing of the plate on 3 sides as observed in figure 4. The pressure is monotonically increasing during about 15 minutes for all the tests and produces strain rate lower than $1x10^{-4}$ s^{-1} corresponding to the same order of magnitude as the tensile tests (see table 1).

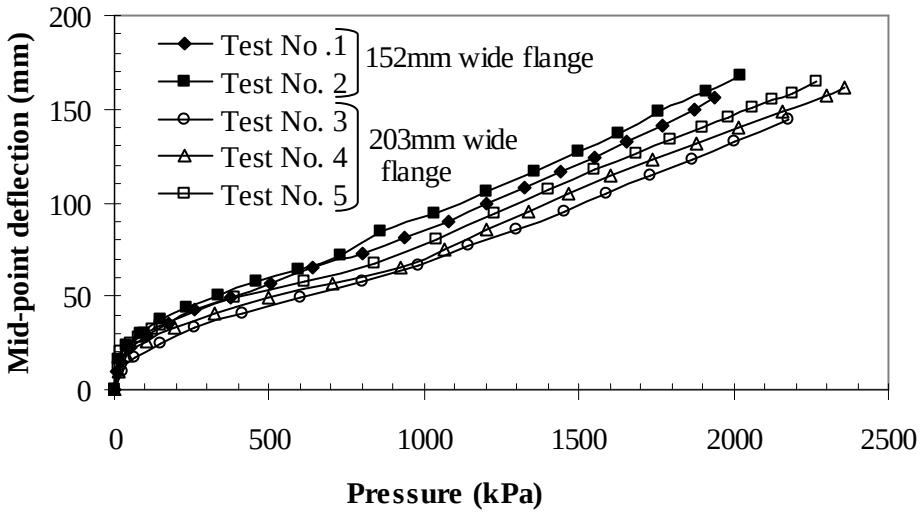

Figure 2: Midpoint deflection for the five plates tested

On some occurrence, the protective coating added over the strain gages cracked as a function of the bending of the plate under the flange. This caused water penetration over the electrical contacts of the gages and their malfunctioning before the failure of the plate. For that reason, test No. 5 used air to pressurize the tank and load the plate. The next section

includes the comparison of the experimental and computed strain.

Table 2: Summary of the experimantal results at failure

Test No.	Exposed area (m^2)	Midpoint deflection (mm)	Pressure at failure (kPa)	Tearing length (mm)
1	3.01	156	1941	1216
2	3.01	167	2019	1162
3	2.83	151	2175	1121
4	2.83	162	2354	1257
5	2.83	165	2265	3 sides

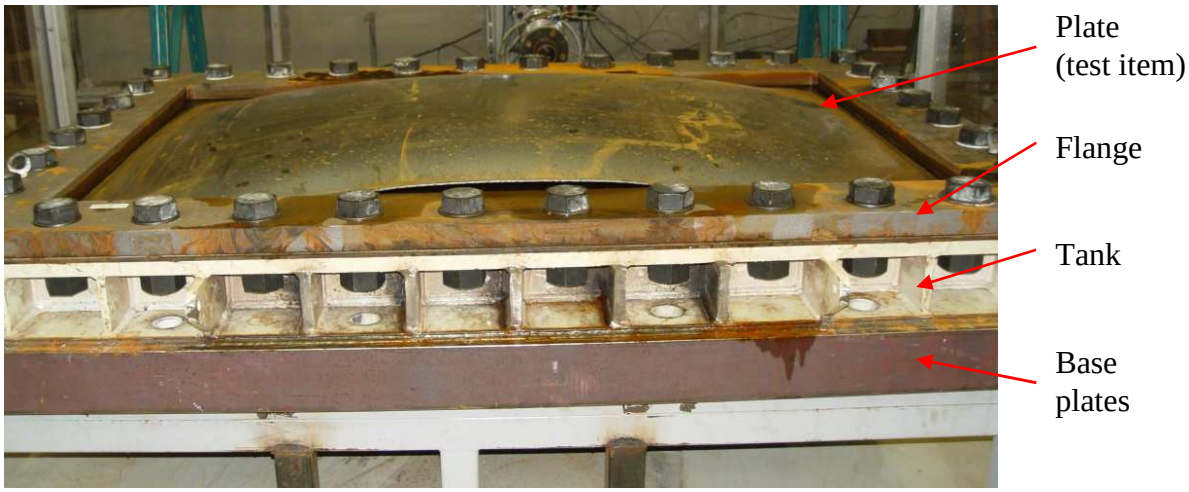

Figure 3: Photograph showing the partial tearing failure (Mode II) of test No. 4

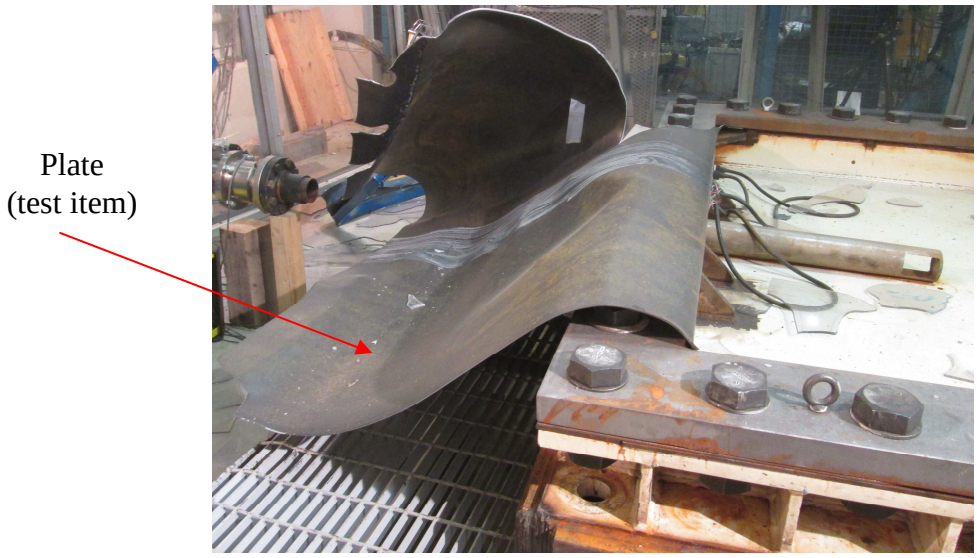

Figure 4: Photograph showing the complete tearing on three sides of the plate for the test No. 5

3 NUMERICAL MODEL

The nonlinear static simulations with large deformation are performed using the Ansys/Mechanical® implicit finite element software. The existence of two planes of reflective symmetry condition allows to model only a quarter of the experimental setup as shown in figure 5. Two FEA models are required to simulate the experimental setup: models A and B simulate the 152 mm and 203 mm wide flanges respectively. The final models do not include the structural base plates of the tank after validating with a coarse mesh that the displacements of the plate and the clamping apparatus were not modified with this exclusion. In this way, the bottom faces of the models are clamped with all displacement and rotational degrees of freedom constrained to zero. A multilinear isotropic hardening model represents the material. The failure criterion is based on the equivalent plastic strain and uses the uni-axial tension test results. The tearing threshold of the plate occurs when the equivalent plastic strain exceeds 14.2 % throughout the thickness of the plate at one point.

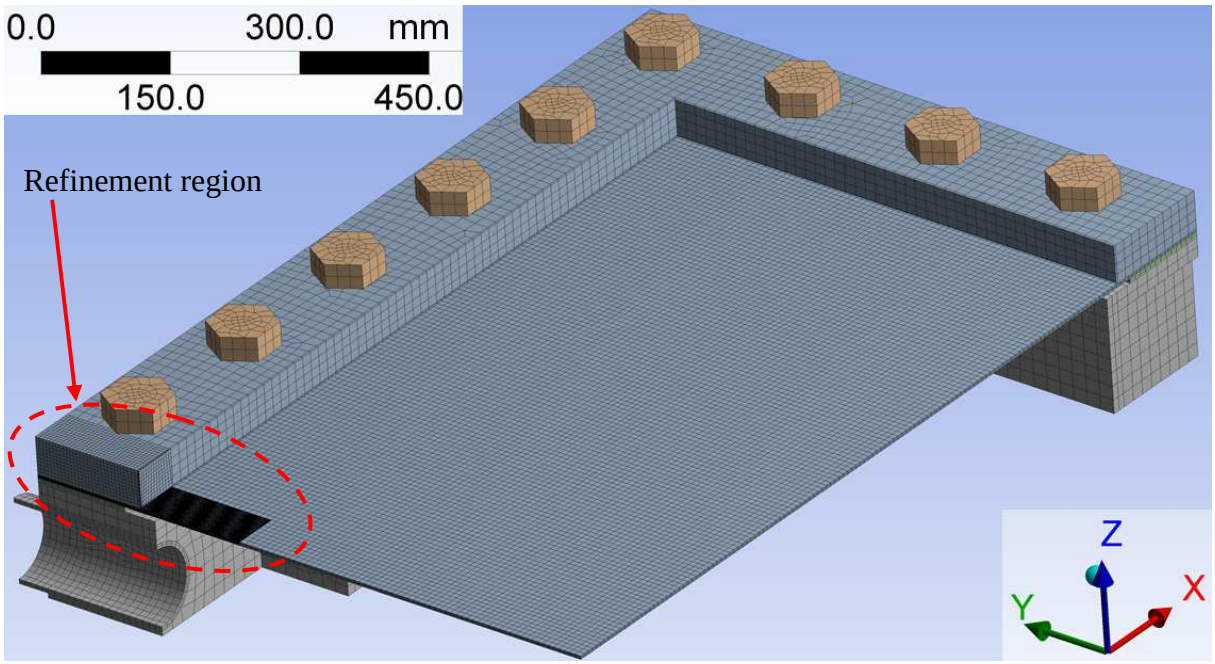

Figure 5: Diagram showing the FEA model A (1/4 of the experimental set up)

The models include frictional contact elements between the top surface of the plate and the flange and also between the bottom surface of the plate and the tank. Twenty-node brick elements are used to model all the parts. A pre-stress analysis is conducted to simulate the bolts pre-tension acting on the assembly.

A convergence-divergence study is executed by successively reducing the size of the elements by a factor of two from 16 to 0.5 mm for the plate's mesh to seek a convergence of the Von Mises stress and the strain component ε_Y. The results retained for this convergence study is at the location of the peak stress under the plate at 181.5 mm of the edge at a pressure of 2000 kPa for FEA model A. This point is located at 4 mm under the flange on the plane of symmetry of the X axis. The number of elements through thickness increases from 2 to 10

during the convergence study to retain suitable aspect ratios. This refinement is only applied in the region of interest of the plate to minimize the size of the FEA models.

Defining the sizes d_i of meshes resulting from 2 successive refinements from mesh size d_{m1} as:

$$d_{m3} = d_{m2}/2 = d_{m1}/4 \tag{1}$$

the stress of interest σ is said to be converging if the two following requirements are respected:

$$\begin{aligned} |\sigma_{m2} - \sigma_{m1}| &> |\sigma_{m3} - \sigma_{m2}| \\ (\sigma_{m2} - \sigma_{m1})(\sigma_{m3} - \sigma_{m2}) &> 0 \end{aligned} \tag{2}$$

According to Sinclair et al. [3], a converged solution is obtained if the following criterion is met:

$$|\sigma_{m3} - \sigma_{m2}| / |\sigma_{m2}| < e_r \tag{3}$$

where e_r, the relative error level, is set to 5% in the present study and corresponds to a good level of confidence. Figure 6 shows the evolution of the Von Mises stress and the strain component ε_Y against the mesh size. For the Von Mises stress, the computation of equation (2) results in a convergence using mesh sizes of 16, 8 and 4 mm as well as for smaller sizes. The calculation of equation (3) gives converged values of stress for meshing of 2 mm and smaller.

For the component strain ε_Y, the convergence is obtained for a mesh size of 2 mm using equation (2) and the values of the strain are converged for mesh sizes of 1 mm and smaller using equation (3). From this point on, all the numerical results presented are obtained from the 0.5 mm mesh with 10 elements trough the thickness in the refinement zone for both FEA models.

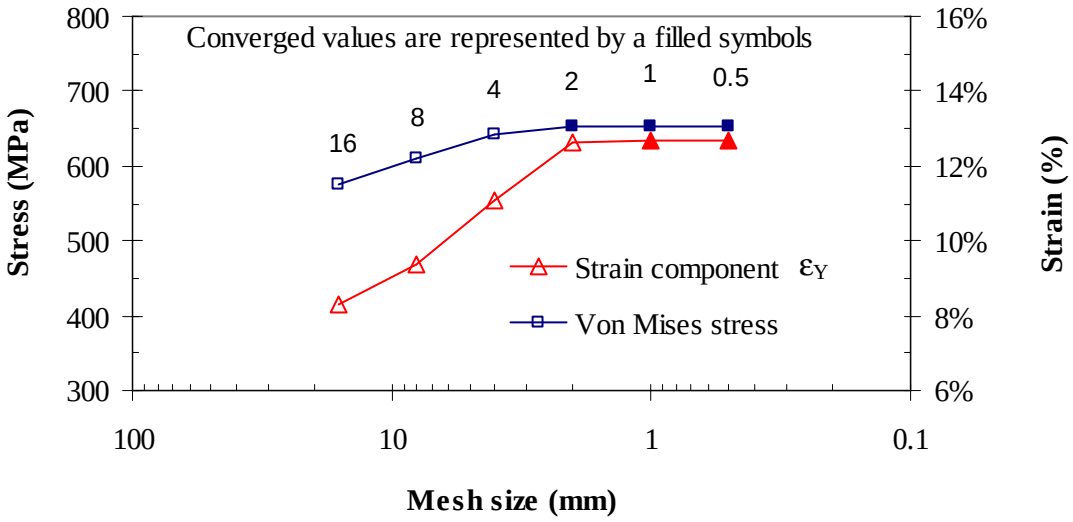

Figure 6: Convergence study on the bottom surface of the plate at 2000 kPa for FEA model A

Comparisons of measured and computed strain are performed at 2 points of interest. First, figure 7 compares the strain from grid No. 2 of the gages installed under the plate (figure 1) and the calculated strain component ε_Y from the numerical models at a pressure of 1000 kPa on the plane of symmetry of the X axis. There is not enough data to establish the experimental distribution of strain at higher pressure. The strain component ε_Y is used for simplicity as the principal strain direction is aligned with the Y axis within ±3 degrees at that location. The calculated strain is obtained by averaging the strain of the nodes covering an area similar to the grid gage to enabled comparison with strain gages. The position of the gages is normalized with the vertical side of the flange facing the center of the plate to compare all experimental results. FEA model B produces less strain than model A for a given pressure owing to the smaller exposed area and the stiffened flange. A different behavior is observed in the experimental results where the strain component ε_Y is larger for the 203 mm wide flange at a normalized distance of around 6 mm under the flange (negative value on the X axis as the face of the flange is positioned at the origin). The malfunctioning of some strain gages as explained earlier reduces the number of experimental data. Also, one point measured on the test No. 5, which was air pressurized, is much larger than the numerical simulation.

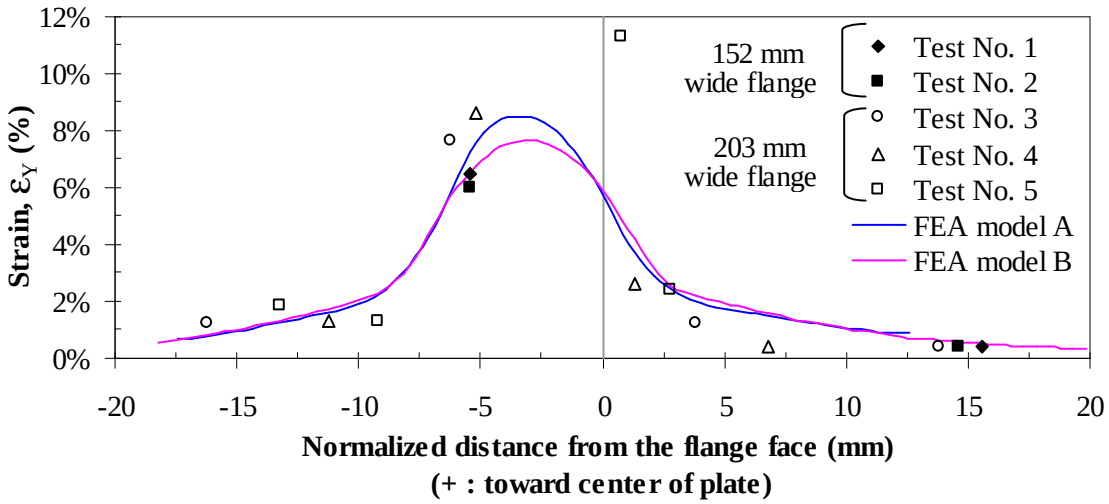

Figure 7: Distribution of the strain component ε_Y on the bottom surface of the plate at 1000 kPa

Next, the evolution of the strain component ε_Y at the center of the plate where membrane strain dominates is shown against the internal pressure in figure 8 for both FEA models and test No. 1, 2 and 3 (there were no strain gage at that location for the other two tests). The direction of the principal strain is aligned with the Y direction at that location. The FEA models capture with a good accuracy the evolution of the experimental strain.

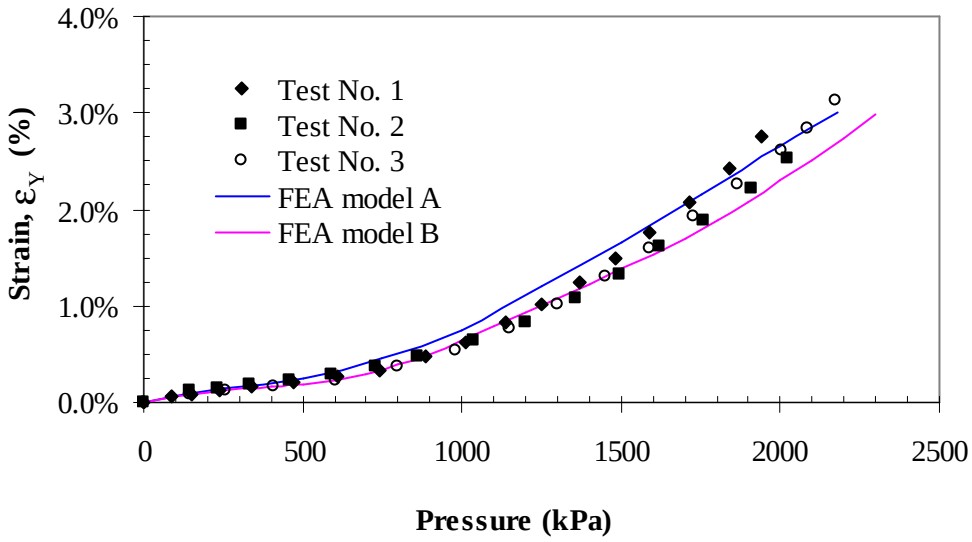

Figure 8: Evolution of the strain component ε_Y at the center of the plate

In our model, the failure of the plate is assumed when the equivalent plastic strain exceeds the failure criterion throughout the plate thickness as illustrated in figure 9 and 10 for the FEA models A and in B respectively. The curved boundary on the flange prevents indentation and some thinning of the plate is observed. Table 3 compares the pressure and the midpoint displacement of the plate at failure. There is an excellent agreement of the deflection of the plate and fairly good correlation of the pressure at failure but the numerical simulation overestimates the pressure at failure in all the cases. This result confirms the observation made on figure 7 were the peak strain is underestimates by the FEA models at 1000 kPa.

The selected failure criterion ε_f is based on a constant equivalent strain and uses the uni-axial tension test results. This criterion has no relationship to the stress triaxiality parameter η, defined as the ratio of the hydrostatic stress to the equivalent stress. Ductility is affected by this parameter and the strain to failure is reduced in the case of positive hydrostatic stress [7][8]. The triaxiality parameter η increases as the state of stress changes from uni-axial tension state ($\eta = 1/3$) to the plane strain state ($\eta = 1/\sqrt{3} = 0.577$) and finally to the equi-biaxial tension state ($\eta = 2/3$). The boundary of the plate at the failure location creates a plane strain state and confirmed by the computation of the parameter η on the bottom face of the plate near the flange where η is constant at 0.56 from the beginning of the loading until the failure [9]. Tension tests at various triaxiality would be required to establish the relation between the strain to failure and the triaxiality specific to the 50W steel as this parameter reduces the pressure to failure in the present study.

Table 3: Comparaison between experimental and numerical results

Test No.	FEA model	Pressure at failure (kPa)			Midpoint deflection at failure (mm)		
		Experimental	FEA	% Diff.	Experimental	FEA	% Diff.
1	A	1941	2170	12%	156	154	-1%
2	A	2019	2170	7%	167	154	-8%
3	B	2175	2520	16%	151	156	3%
4	B	2354	2520	7%	162	156	-4%
5	B	2265	2520	11%	165	156	-5%

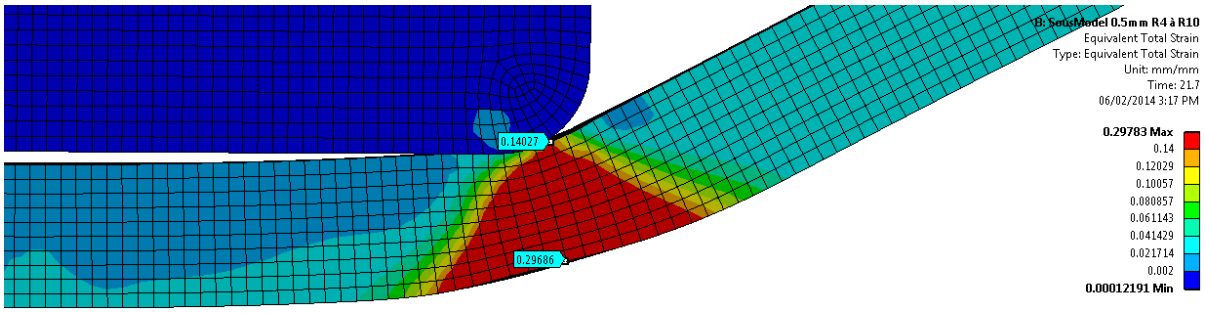

Figure 9: Strain plot of a section of the plate under the flange showing failure at 2170 kPa for FEA model A

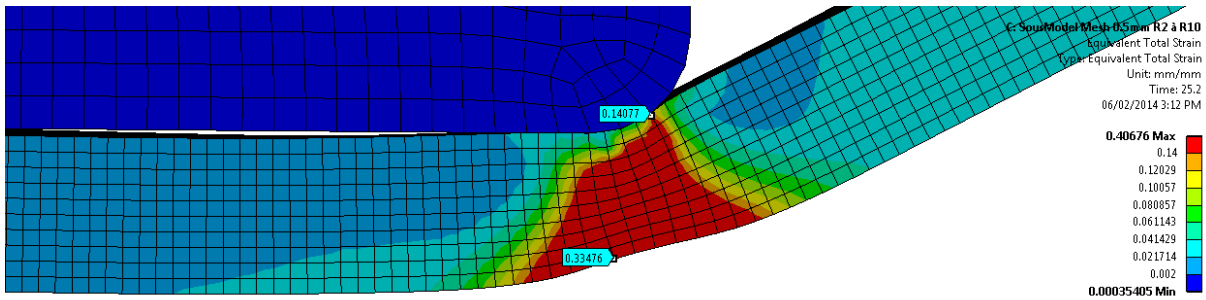

Figure 10: Strain plot of a section of the plate under the flange showing failure at 2520 kPa for FEA model B

12 CONCLUSIONS

In the present paper, the behavior of large steel plates loaded until failure was presented and compared to numerical simulations. A good agreement was observed between the computed maximum plate deflection and the experimental results. Good correlation with the strain gauges measurements was also observed in areas where membrane strain dominates. Comparison of the computed strain near the flange where bending strain dominates was less satisfactory owing to the high strain gradient in this area. The predicted failure of the plates is overestimated from 7% to 16%. A convergence study has shown that relatively small mesh size is required compared with the plate's dimensions to obtain a converged solution.

REFERENCES

[1] Houlston, R., Slater, J.E., Pegg, N., DesRochers, C.G., On analysis of structural response of ship panels subjected to air blast loading, *Computer & Structures* (1985) **21**:273-289.

[2] Menkes, S.B, Opat, S.B., Tearing and shear failures in explosively loaded clamped beams, *Experimental. Mech*anica (1973) **13**:480-486.

[3] Sinclair, G.B., Beishem, J.R., Sezer, S., Practical convergence-divergence checks for stresses from FEA, *Proceedings of the 2006 International ANSYS Conference* (2006), p.50

[4] Nurick, G.N., Gelman, M.E., Marshall, N.S., Tearing of blast loaded plates with clamped boundary conditions, *Int. J. of Impact Engineering* (1996) **18** Nos 7-8: 803-827.

[5] Sinclair, G.B., Stress singularities in classical elasticity – I: Removal, interpretation, and analysis, *Applied Mechanics Reviews* (2004) **57** No 4:251-297.

[6] Yuan, Y., Tan, P.J., Deformation and failure of rectangular plates subjected to impulsive loadings, *Int. J. of Impact Engineering* (2013) **59**:40-52.

[7] Rice, J.R., Tracey, D.M., On the ductile enlargement of voids in triaxial stress fields, *Journal of the Mechanics and Physics of Solids* (1969) **17**:201-217.

[8] Hancock, J.W., Mackenzie, A.C., On the mechanisms of ductile failure in high-strength steels subjected so multi-axial stress-states, *J. Mech. Phys. Solids* (1976) **24**:147-169.

[9] Wierzbicki, T., Bao, Y., Lee, Y.W., Bai, Y., Calibration and evaluation of seven fracture models, *Int. J. of Mechanical Sciences* (2005) **47**:719-743.